The Astrophysical Journal, 677:249–261, 2008 April 10

SPATIALLY RESOLVED IMAGING AT 350 μm OF COLD DUST IN NEARBY ELLIPTICAL GALAXIES

Lerothodi L. Leeuw,[1,2,3] Jacqueline Davidson,[4] C. Darren Dowell,[5] and Henry E. Matthews[6]

Received 2007 June 24; accepted 2007 December 18

ABSTRACT

Continuum observations at 350 μm of seven nearby elliptical galaxies for which CO gas disks have recently been resolved with interferometry mapping are presented. These SHARC II mapping results provide the first *clearly resolved* far-infrared (FIR)–to–submillimeter continuum emission from cold dust (with temperatures 31 K $\gtrsim T \gtrsim$ 23 K) of any elliptical galaxy at a distance >40 Mpc. The measured FIR excess shows that the most likely and dominant heating source of this dust is not dilute stellar radiation or cooling flows, but rather star formation that could have been triggered by an accretion or merger event and fueled by dust-rich material that has settled in a dense region cospatial with the central CO gas disks. The dust is detected even in two cluster ellipticals that are deficient in H I, showing that, unlike H I, cold dust and CO in ellipticals can survive in the presence of hot X-ray gas, even in galaxy clusters. No dust cooler than 20 K, either distributed outside the CO disks or cospatial with and heated by the entire dilute stellar optical galaxy (or very extended H I), is currently evident.

Subject headings: galaxies: elliptical and lenticular, cD — galaxies: ISM — galaxies: photometry — infrared: galaxies — radio continuum: galaxies — submillimeter

1. INTRODUCTION

Cold gas and dust in nearby elliptical galaxies were detected only fairly recently (Sadler & Gerhard 1985; Knapp et al. 1989; Lees et al. 1991; Wiklind & Henkel 1995). Compared to that in spiral galaxies, the cold interstellar medium (ISM) in ellipticals is present in relatively small amounts and is seen in only 50%–80% of nearby ellipticals. The source and content of the cold ISM in these galaxies is still uncertain, with optical and far-infrared (FIR) dust mass estimates differing by $\sim$10–100 (e.g., Goudfrooij & de Jong 1995).

There is some evidence for an internal origin of the dust arising in circumstellar envelopes of red giant stars. This internal origin is supported by the detection of $\sim$10 μm emission in excess of the stellar emission, with the same de Vaucouleurs profile as the optical stellar images and near- to mid-infrared photospheric emission (e.g., Athey et al. 2002). Some have suggested that this dust will come in contact with the hot ISM ($\sim 10^7$ K) and be eroded in thermal collisions with ions and destroyed in only $\sim 10^7$–10^8 yr (e.g., Schweizer 1998). However, Mathews & Brighenti (2003) have argued that the dust may induce efficient cooling of the hot gas on a timescale shorter than the destruction lifetimes of the dust in the hot gas, allowing some dust to survive and settle primarily in the centers of the galaxies while the hot gas cools. They propose that if this dust-induced cooling is the dominant evolutionary path of the dust from stars, the thermal energy released by the hot ISM should be reradiated by dust in the FIR and could be responsible for the central dusty disks and clouds seen in ellipticals.

It has also been suggested that mergers or accretion events that include a gas-rich galaxy may be the dominant source of dust in ellipticals. The total FIR luminosities (e.g., Temi et al. 2004) and cold gas content (Knapp et al. 1985; Lees et al. 1991) of ellipticals are observed to be uncorrelated with their optical luminosities. This lack of correlation, together with *HST* detections of irregular dust lanes and filaments with random orientations with respect to the optical major axes (e.g., Tran et al. 2001), is usually interpreted as evidence that the dust has been externally acquired. The external origin is likely to be accretion via the interaction of an elliptical galaxy with a gas-rich spiral or in mergers of gas-rich spirals that evolve through an FIR-bright (starburst) phase as they relax to form ellipticals (e.g., Toomre & Toomre 1972; Schweizer 1998). In fact, if elliptical galaxies are formed through spiral mergers, then starbursts are necessary to produce the high phase-space densities seen in the centers of elliptical galaxies (e.g., Rothberg & Joseph 2004 and references therein). Numerical simulations by Barnes (2002) have shown that 20%–60% of the gas from two spirals merging can form relaxed disks of sizes up to 20 kpc, with some of the gas possibly losing angular momentum, falling to the nucleus of the galaxy, and perhaps leading to star formation.

Observations of dust emission from elliptical galaxies have been made primarily using *IRAS* or *ISO* (e.g., Knapp et al. 1989; Temi et al. 2004). These measurements favored the warm dust components of the ISM and produced unresolved images of the dust emission. The *IRAS*- and *ISO*-derived SEDs of these galaxies clearly show that there are multitemperature components to the dust. Indeed, the presence of an additional, low-level, very cold (<20 K) dust component in ellipticals has been suggested by limited detections of unresolved millimeter and submillimeter emission in some nearby galaxies (Knapp & Patten 1991; Wiklind et al. 1995; Leeuw et al. 2004; Temi et al. 2004), as well as clearly extended FIR-to-submillimeter detections from the dust lane in the nearest giant elliptical galaxy, NGC 5128, that hosts the active galactic nucleus (AGN) Centaurus A (e.g., Leeuw et al. 2002; Quillen et al. 2006). Observations of CO emission from a number of ellipticals show that many of them contain significant amounts of molecular gas (Lees et al. 1991; Wiklind & Henkel 1995), but many of these observations do not spatially resolve the CO emission.

[1] Department of Physics and Electronics, Rhodes University, P.O. Box 94, Grahamstown 6140, South Africa; lerothodi@alum.mit.edu.
[2] South Africa Square Kilometre Array/MeerKAT, Lonsdale Building, Lonsdale Road, Pinelands 7405, South Africa; lerothodi.leeuw@ska.ac.za.
[3] Space Science and Astrophysics Branch, NASA Ames Research Center, MS 245-6, Moffett Field, CA 94035; lerothodi.l.leeuw@arc.nasa.gov.
[4] USRA-SOFIA, NASA Ames Research Center, MS 211-3, Moffett Field, CA 94035; jdavidson@sofia.usra.edu.
[5] Jet Propulsion Laboratory, California Institute of Technology, MS 169-506, 4800 Oak Grove Drive, Pasadena, CA 91109; charles.d.dowell@jpl.nasa.gov.
[6] Herzberg Institute of Astrophysics, National Research Council of Canada, P.O. Box 248, Penticton, BC V2A 6J9, Canada; henry.matthews@nrc-cnrc.gc.ca.

TABLE 1
PUBLISHED OPTICAL AND MOLECULAR GAS PROPERTIES OF THE ELLIPTICALS

Source	Type	Environment, Notables, and Merger or Accretion Stage	$M(H_2)$ ($10^8\ M_\odot$)	M(H I) ($10^8\ M_\odot$)	D (Mpc)	L_B ($10^9\ L_\odot$)	$(B-V)_e$ (mag)
NGC 3656	Ep	Early-age major merger/accr.?	47	11	45	16	...
NGC 5666	cE2/SO	Intermediate merger/accr.?	5.7	10	35	6	0.86
NGC 83	E0	Group member, late merger/accr.?	20	...	85	44	1.12
NGC 759	E0/1	Cluster A262, late merger/accr.?	24	<24	66	34	1.05
NGC 807	E3	Field, quiescent/very late accr.?	14	61	64	31	0.97
UGC 1503	E1	Field, quiescent/very late accr.?	18	16	69	16	...
NGC 4476	dE5p/SO	Virgo Cluster, dwarf merger/accr.?	1.1	<1	18	3	0.85

NOTE.—Adopted from Murray et al. (2000), Tomita et al. (2000), Wiklind et al. (1995, 1997), Young (2002, 2005) and references therein.

Recently, interferometric measurements by Young (2002, 2005) and Wiklind et al. (1997) have spatially resolved the CO(1–0) emission in seven elliptical galaxies with spatial resolutions of 7″ and 3″, respectively. These data imply that the molecular gas is contained mostly in rotating disks lying within the central 5 kpc of the galaxies. This prompted the study by our group to spatially resolve the dust emission in these seven elliptical galaxies. Our goals were (1) to determine the physical properties of the dust coincident with the molecular gas, (2) to see if there are dust associations with other spatial distributions (e.g., stellar distribution), and (3) to determine the most likely heating source (or sources) for the dust. We also wanted to address the question of whether these observed gas disks are the result of external merger/accretion events, as suggested by the optical morphological signatures of the galaxies, or internal mass-losing stars that constitute their elliptical optical components.

The seven galaxies in our sample (NGC 83, NGC 759, NGC 807, UGC 1503, NGC 3656, NGC 4476, and NGC 5666) were all classified by Wiklind & Henkel (1995) as ellipticals, based on the determination that their luminosity profiles follow the $R^{-1/4}$ de Vaucouleurs law. However, morphologically, the sample includes galaxies from different extragalactic environments and represents a spread of possible merger/accretion tracers or ages, from galaxies that have been classified as ongoing or early-age major mergers (e.g., NGC 3656; Balcells et al. 2001) to very late accretion or quiescent systems (e.g., NGC 807; Murray et al. 2000). Recent CCD imaging of some of the galaxies, e.g., NGC 5666 by Donzelli & Davoust (2003), have disputed the classification as ellipticals in favor of SO galaxies, while new optical observations of others, e.g., NGC 83 by Young (2005), have confirmed the elliptical classification.

The sample's updated environments, general properties, and molecular gas content are summarized in Table 1. The observational merger or accretion signatures of the sample are worthy of note, as they fortuitously allow an evolutionary analysis in the context of merger/accretion stages and cold dust and gas properties. These merger/accretion signatures are described further with other observational characteristics of the galaxies in § 3.

2. MAPPING OBSERVATIONS USING SHARC II AT 350 μm

We observed NGC 83, NGC 807, UGC 1503, and NGC 759 with SHARC II on 2005 October 11–14 and NGC 3656, NGC 4476, and NGC 5666 on 2006 April 23 and 29. SHARC II has a 12×32 bolometer array with an instantaneous field of view of $148'' \times 56''$. We achieved background subtraction and mapping coverage for the galaxies by having the telescope execute a Lissajous scanning pattern with amplitude 60″ in azimuth and 40″ in elevation. During the observations we maintained a log of air mass and zenith water vapor, the telescope dish segments were kept in optical alignment using the Caltech Submillimeter Observatory (CSO) Dish Surface Optimization System, and pointing calibrations were executed every hour, allowing us to achieve a FWHM beam size of 8.5″ and pointing accuracy of about 2″ rms. The zenith atmospheric opacity at 225 GHz, during the observations and as measured by the CSO facility radiometer, varied from 0.04 to 0.06.

For flux calibration we observed Callisto, Uranus, CRL 618, CRL 2688, Vesta, Arp 220, CIT 6, Neptune, or *o* Cet hourly. The assumed fluxes for the exosolar calibrators are 10.2 Jy beam^{-1} for Arp 220, 19.4 Jy beam^{-1} for CRL 618, 2.33 Jy beam^{-1} for *o* Cet, 41.6 Jy beam^{-1} for CRL 2688, and 2.42 Jy beam^{-1} for CIT 6; for the solar system calibrators in October, 232 Jy beam^{-1} for Uranus, 90.0 Jy beam^{-1} for Neptune, and 5.77 Jy beam^{-1} for Vesta; and in April, 95.8 Jy beam^{-1} for Callisto. The absolute calibration uncertainty is estimated to be 20%.

The SHARC II contour maps are shown in Figures 1–7 and are the result of about 3.0 hr of observing on NGC 83, 7.4 hr on NGC 807, 6.3 hr on UCG 1503, 2.3 hr on NGC 759, 1.9 hr on NGC 3656, 2.4 hr on NCG 4476, and 1.3 hr on NGC 5666. The data were analyzed using the SHARC II reduction software SHARCSOLVE, which iteratively solves for the source image, atmospheric background, and detector gains and offsets. During the iterations a constraint was applied in the map domain: outside a diameter of 37″ or 46″, the source image was assumed to be zero. The 46″ diameter was applied to the maps of NGC 807 and UGC 1503, and the 37″ diameter was applied to those of the other sources. The positional accuracies of the galaxies are based on the pointing observations of the calibration sources. However, to optimize the effective resolution, the co-added images are composed of hour-long subimages whose centroids have been aligned. This relative alignment was performed for all objects except NGC 807 and UGC 1503, which were too faint and extended to have well-defined centroids after 1 hr integrations. The 350 μm fluxes of these maps are given in Table 2. The integrated fluxes were obtained in a 46″ aperture for NGC 807 and UGC 1503 and a 37″ aperture for all the other target objects.

3. SUBMILLIMETER MORPHOLOGY VERSUS OBSERVATIONS FROM OTHER WAVE BANDS

The goal of this submillimeter wavelength study is to directly map the emission from cold dust that may be cospatial with the optical dust features and/or the CO gas disks presented by Wiklind et al. (1997) and Young (2002, 2005) for the sample galaxies, as well as any emission from dust not detected by the optical and

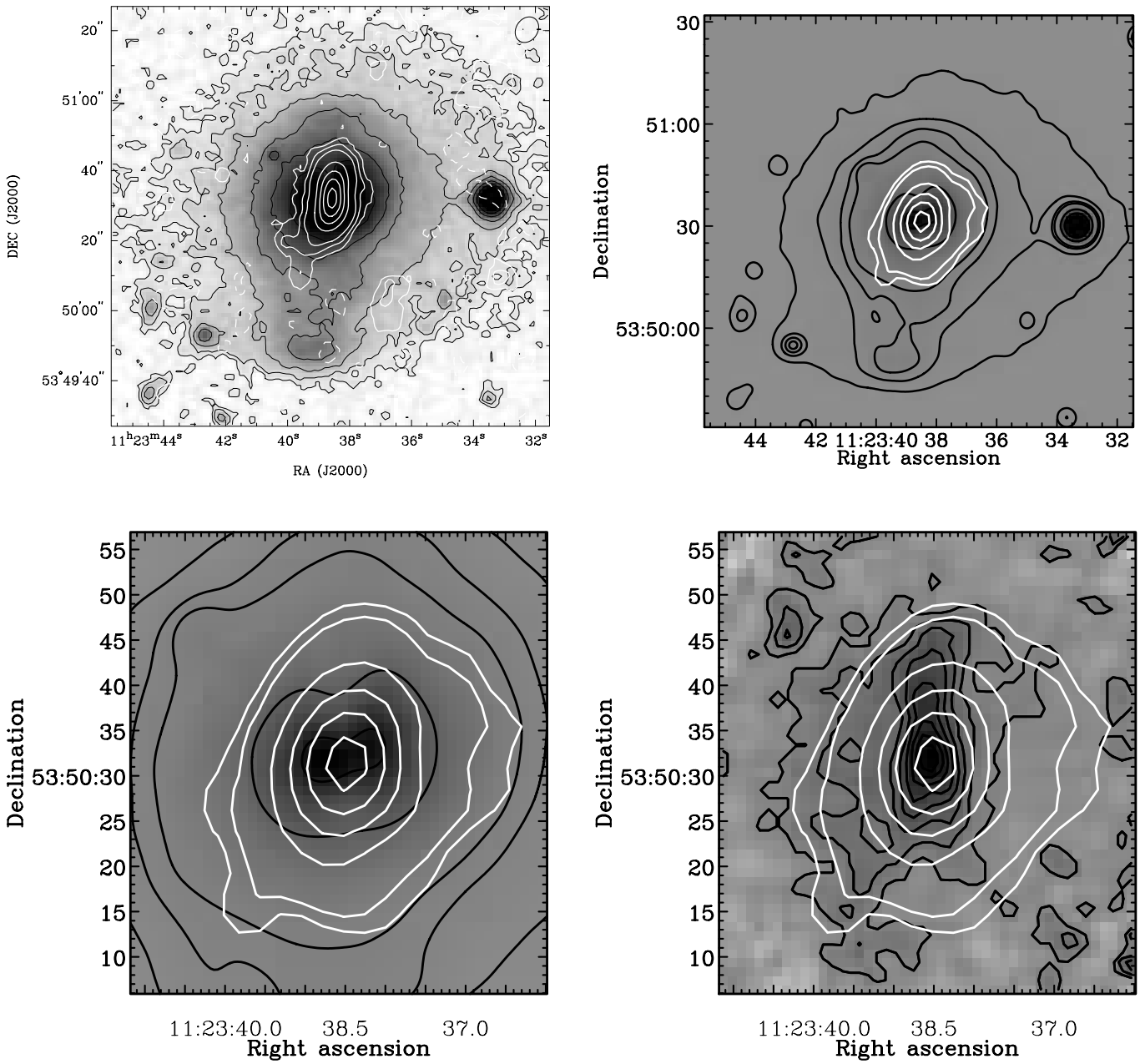

FIG. 1.— *Top left*: Total integrated CO(1–0) intensity map of NGC 3656 (*white contours*), with a measured 10% contour level diameter of 34″, overlaid on the gray scale and black contours from the red part of the optical DSS2, as presented by Young (2002). The white contours are in units of −5%, −2%, 2%, 5%, 10%, 20%, 30%, 50%, 70%, and 90% of 81.1 Jy beam^{-1} km s^{-1} = 4.7×10^{22} cm^{-2} CO peak (Young 2002). *Top right*: CSO/SHARC II 350 μm continuum smoothed to 10″ (*white contours*), overlaid on intensity gray scale and black contours of the SDSS *i*-band image of NGC 3656 smoothed to 10″. The SDSS *i*-band and submillimeter contours are, respectively, ∼57%, 58%, 59%, 60%, 70%, and 90% and 10%, 30%, 50%, 70%, and 90% of the maximum pixel values on the maps and are intended to display areas that may be cospatial with the CO as shown in the top left panel. *Bottom left*: Zoom-in of the top right panel. *Bottom right*: CSO/SHARC II 350 μm continuum smoothed to ∼10″ (*white contours*), overlaid on gray scale and black contours of the SDSS $i - g$–band images smoothed to 2″. The SDSS contours are on a linear scale, and the submillimeter contours are as above. In the SDSS $i - g$–band maps, darker pixels have redder colors.

CO studies. The presented submillimeter mapping is sensitive to continuum emission from optically thin dust; thus, the observations will detect emission from dust that may be deep or in the far side of the galaxies and therefore not easily visible in the optical images. The detected submillimeter distribution and fluxes are analyzed to assess their galactic associations and the possible mechanisms heating the dust; therefore, the submillimeter mapping spatially and physically probes the dust's origin, in conjunction with observations at other wavelengths.

Below, the distributions of the mapped submillimeter emission are compared to those of galactic components observed at other wavelengths. In § 5 the observed submillimeter fluxes are used to calculate and analyze the heating of dust by star formation and other possible submillimeter-emitting galactic sources.

Figures 1–7 show the contours of the detected 350 μm dust continuum for the sample and the total integrated CO(1–0) intensity maps from Young (2002, 2005) and Wiklind et al. (1997) overlaid on the optical Sloan Digital Sky Survey (SDSS) maps and, where there are no SDSS images available, on the Digitized Sky Survey 2 (DSS2) images. The SDSS images have more reliable photometry than the DSS2 images, and the SDSS images are plotted convolved to a 10″ beam similar to that of the CSO dust emission images, while the DSS2 images are plotted at their full resolution. Figures 1, 2, and 7 also show SDSS $i - g$–band

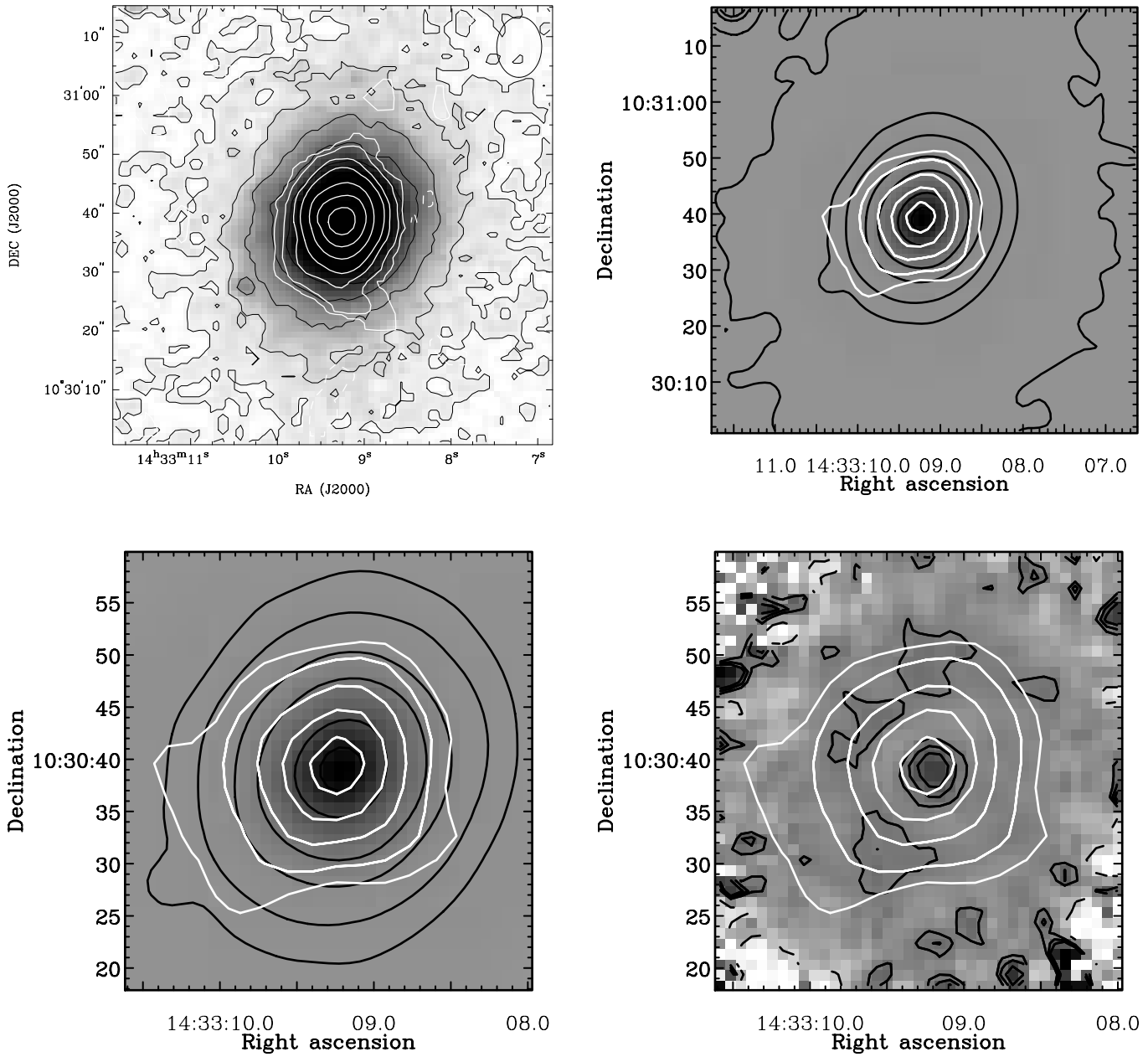

FIG. 2.—*Top left*: Total integrated CO(1–0) intensity map of NGC 5666 (*white contours*), with a measured 10% contour level diameter of 26″, overlaid on the gray scale and black contours from the red part of the optical DSS2, as presented by Young (2002). The white contours are in units of −10%, −5%, 5%, 10%, 20%, 30%, 50%, 70%, and 90% of 21.3 Jy beam^{-1} km s^{-1} = 7.5×10^{21} cm^{-2} CO peak (Young 2002). *Top right*: CSO/SHARC II 350 μm continuum smoothed to 10″ (*white contours*), overlaid on the intensity gray scale and black contours of the SDSS *i*-band image of NGC 5666 smoothed to 10″. The SDSS *i*-band and submillimeter contours are, respectively, ∼40%, 41%, 42%, 45%, 50%, 70%, and 90% and 20%, 30%, 50%, 70%, and 90% of the maximum pixel values on the maps and are intended to display areas that may be cospatial with the CO as shown in the top left panel. *Bottom left*: Zoom-in of the top right panel. *Bottom right*: CSO/SHARC II 350 μm continuum smoothed to ∼10″ (*white contours*), overlaid on the gray scale and black contours of the SDSS $i - g$–band images smoothed to 2″. The SDSS contours are on a linear scale, and the submillimeter contours are as above. In the SDSS $i - g$–band maps, darker pixels have redder colors.

color or extinction maps and their linear contours in an attempt to show some of the dust's geometry. For a smooth presentation, these color maps are shown convolved to a 2″ beam.

The SDSS and DSS2 intensity contours are percentages of the respective peaks in the maps and are intended to display areas that may be cospatial at different wavelengths. The 50% contour level diameters determined by eye from these plots after deconvolution are listed in Table 3. For NGC 3656 the optical 50% contour level diameter is well off the maps plotted in Figure 1, and therefore only the optical 70% contour level diameter is listed in Table 3. These tabulated image sizes were derived after deconvolving beam sizes of 7″ for the CO images (except for the size of NGC 759, where a 3″ beam was used) and 10″ for the submillimeter and SDSS images. For the submillimeter and SDSS images, the diameter measurements done by eye were compared with FWHM diameters from two-dimensional Gaussian fits assuming elliptical shapes and agreed to within ∼5%. For the DSS2 images, the diameters listed are from the full-resolution maps. The relative-percentage contours of the optical maps will be affected by the distribution of dust in these galaxies. Therefore, the optical intensity contours on those maps are not a simple reflection of the stellar distributions as shown on those maps and listed in Table 3; rather, they show the stars plus their attentuation by internal galactic dust of varying distributions, and for the DSS2

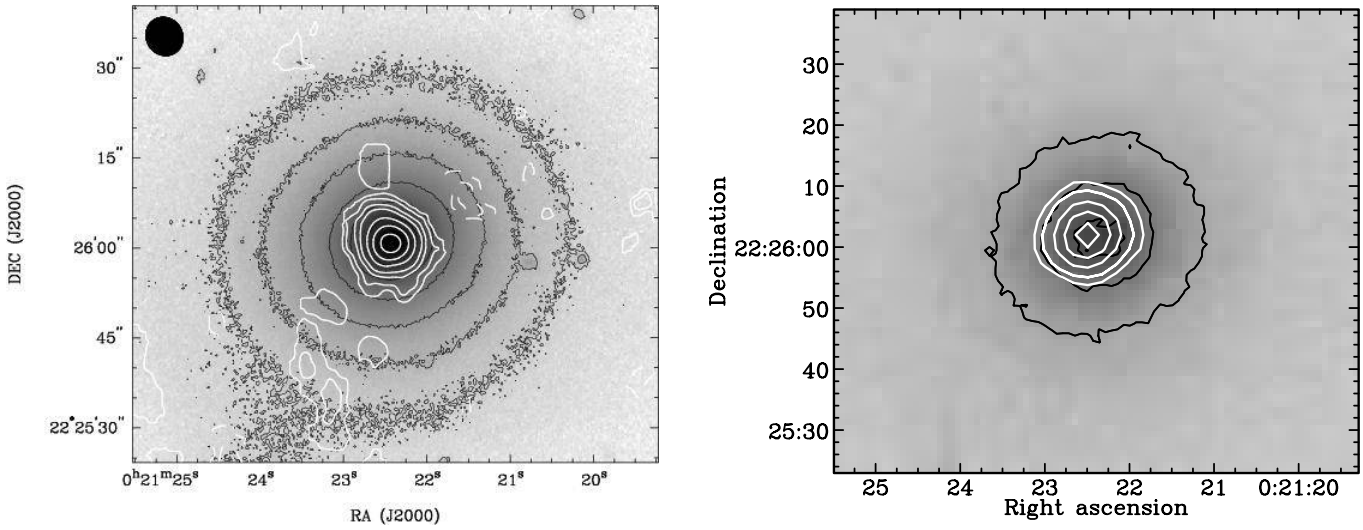

FIG. 3.—*Left*: Total integrated CO(1–0) intensity map of NGC 83 (*white contours*), with a measured 10% contour level diameter of 10″, overlaid on the gray scale and black contours from the red part of the optical DSS2, as presented by Young (2005). The white contours are in units of −20%, −10%, 10%, 20%, 30%, 50%, 70%, and 90% of the 12.7 Jy beam^{-1} km s^{-1} = 8.8×10^{21} cm^{-2} CO peak (Young 2005). *Right*: CSO/SHARC II 350 μm continuum smoothed to 10″ (*white contours*), overlaid on the intensity gray scale and black contours of the DSS2 blue image of NGC 83. The DSS2 blue and submillimeter contours are, respectively, 50%, 70%, and 90% and 20%, 30%, 50%, 70%, and 90% of the maximum pixel values on the maps and are intended to display areas that may be cospatial with the CO as shown in the left panel. The DSS2 image of NGC 83 is saturated and plotted only as a guide to the possible optical extent of this galaxy.

images may also show saturation from the original photographic images.

The 350 μm results show that the detected dust continuum of all the presented ellipticals generally follows the extended CO emission that has been previously detected in these galaxies. This is therefore consistent with emission from cold dust that occurs in dense, gas-rich star formation regions, as is commonly seen in mapping observations of the Milky Way and other star-forming galaxies (e.g., Seaquist & Clark 2001) and confirms CO-FIR correlations of unresolved data from elliptical galaxies that have suggested that cold gas and dust coexist in ellipticals (e.g., Lees et al. 1991). Individual galaxies are discussed in the following subsections.

3.1. *The Early-Age Major-Merger/Accretion Elliptical NGC 3656*

Resolved imaging of NGC 3656 by Balcells et al. (2001) showed that H I occurs in shells and tidal tails that are thought to be signatures of a recent (or early-age) major merger of this galaxy. The H I is more extended than the galaxy's main optical component. Sensitive CCD optical images of the dust features in NGC 3656 were studied by Balcells (1997) and Rothberg &

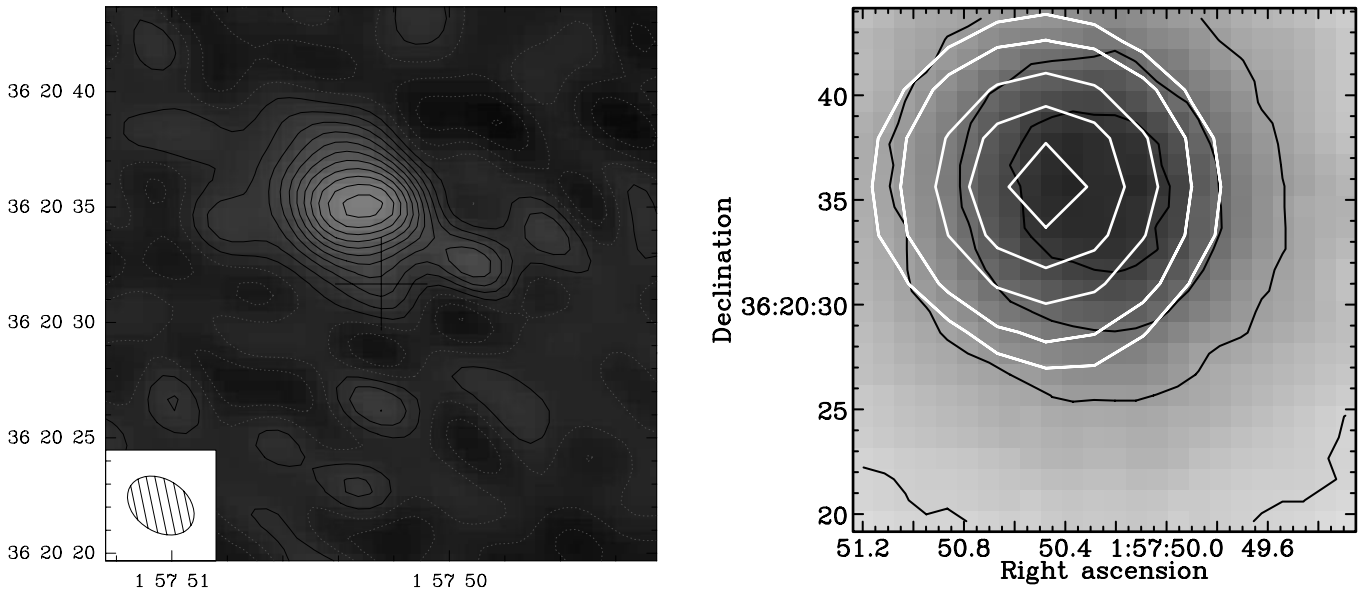

FIG. 4.—*Left*: Total integrated CO(1–0) intensity map of NGC 759 (*gray scale and black contours*) adopted from the paper by Wiklind et al. (1997). The diameters of the CO, black contour level spacing, and rms noise in the map are, respectively, 5″, 0.8 Jy km s^{-1}, and 0.8 Jy km s^{-1} (Wiklind et al. 1997). *Right*: CSO/SHARC II 350 μm continuum smoothed to 10″ (*white contours*), overlaid on the intensity gray scale and black contours of the DSS2 blue image of NGC 759. The DSS2 blue and submillimeter contours are, respectively, 30%, 50%, 70%, and 90% and 20%, 30%, 50%, 70%, and 90% of the maximum pixel values on the maps and are intended to display areas that may be cospatial with the CO as shown in the left panel.

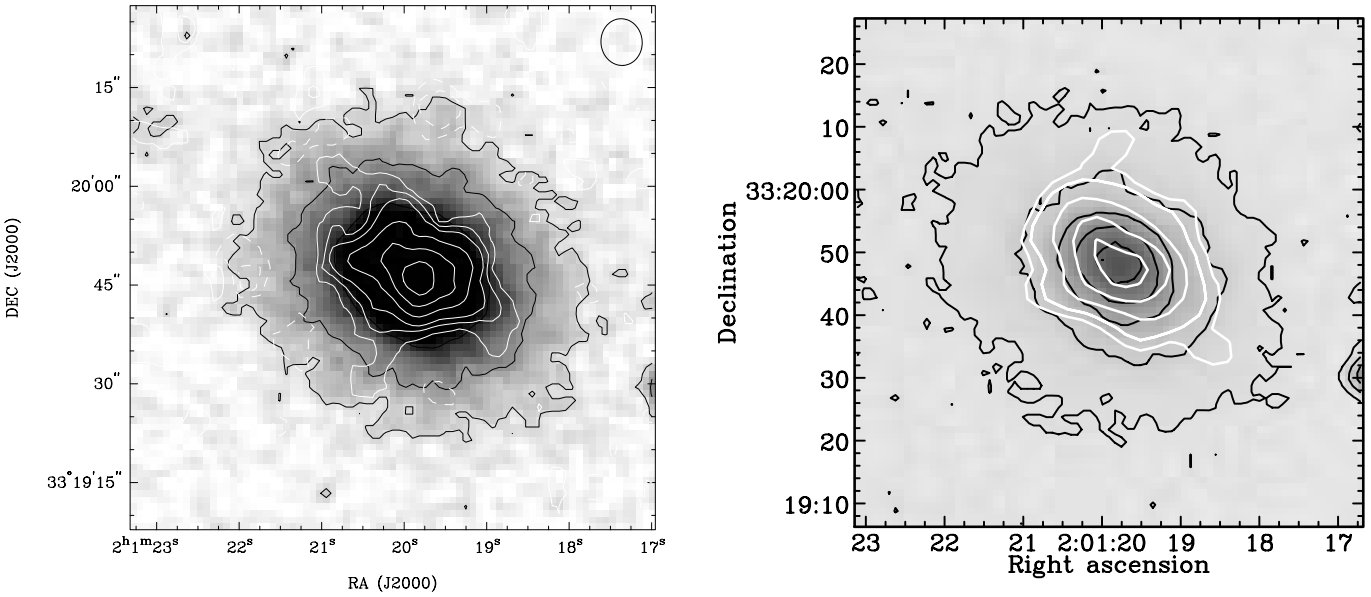

FIG. 5.—*Left*: Total integrated CO(1–0) intensity map of UGC 1503 (*white contours*), with a measured 10% contour level diameter of 30″, overlaid on the gray scale and black contours from the red part of the optical DSS2, as presented by Young (2002). The white contours are in units of −20%, −10%, 10%, 20%, 30%, 50%, 70%, and 90% of 6.3 Jy beam^{-1} km s^{-1} = 3.9×10^{21} cm^{-2} CO integrated intensity peak (Young 2002). *Right*: CSO/SHARC II 350 μm continuum smoothed to 10″ (*white contours*), overlaid on the intensity gray scale and black contours of the DSS2 blue image of UGC 1503. The DSS2 blue and submillimeter contours are, respectively, 20%, 30%, 50%, 70%, and 90% and 20%, 30%, 50%, 70%, and 90% of the maximum pixel values on the maps and are intended to display areas that may be cospatial with the CO as shown in the left panel.

Joseph (2006), who suggest that the dust is a remnant of a dust-rich merger that involved this galaxy's primary optical elliptical component.

Figure 1 shows that large-scale, 350 μm dust continuum spurs in the southeastern part of NGC 3656 generally follow the CO emission and optical spurs respectively presented by Young (2002) and Balcells (1997). The 350 μm continuum spurs also follow the optical spurs shown by Balcells (1997) in the western part of this early-merger galaxy. These spurs may be large-scale features of a warped disk of dust that has been reported in the center of NGC 3656 (e.g., Balcells 1997) and described further below.

Figure 1 also shows that the extinction contours of NGC 3656 are very asymmetric, depicting strong extinction in the galactic east and dense north-south central dust distribution. The dust in

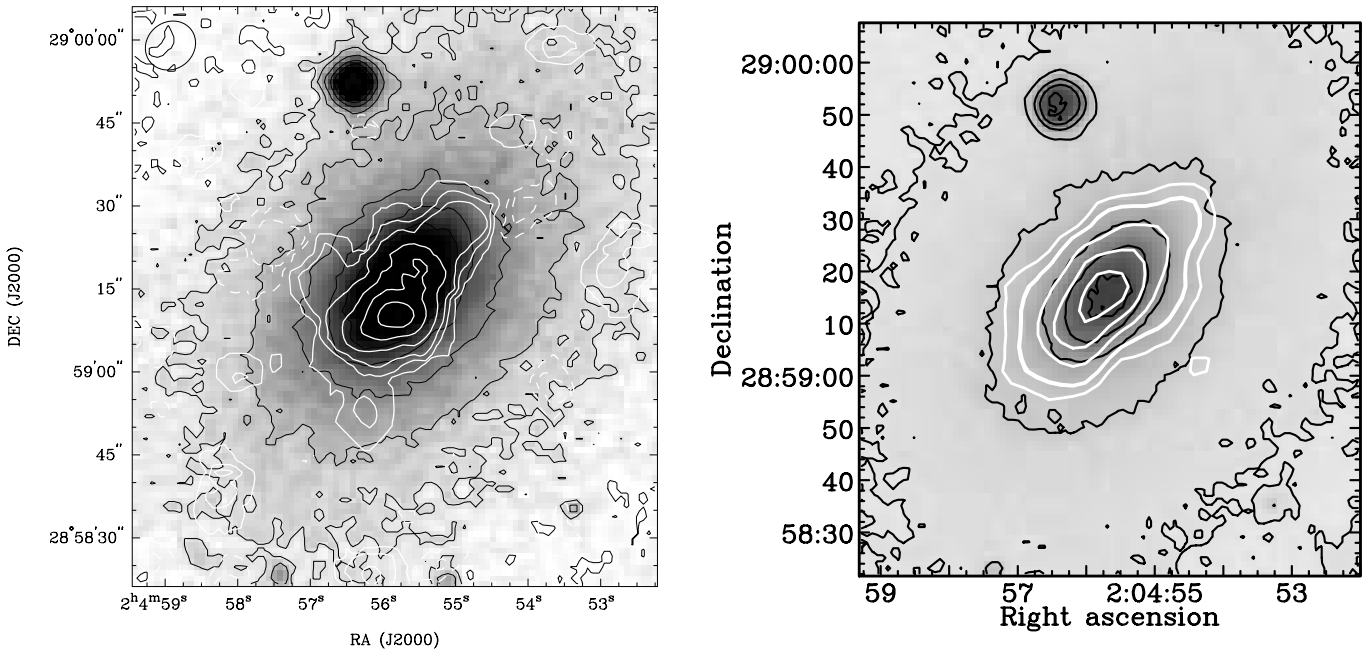

FIG. 6.—*Left*: Total integrated CO(1–0) intensity map of NGC 807 (*white contours*), with a measured 10% contour level diameter of 40″, overlaid on the gray scale and black contours from the red part of the optical DSS2, as presented by Young (2002). The white contours are in units of −20%, −10%, 10%, 20%, 30%, 50%, 70%, and 90% of 7.6 Jy beam^{-1} km s^{-1} = 2.6×10^{22} cm^{-2} CO peak (Young 2002). *Right*: CSO/SHARC II 350 μm continuum smoothed to 10″ (*white contours*), overlaid on the intensity gray scale and black contours of the DSS2 blue image of NGC 807. The DSS2 blue and submillimeter contours are, respectively, 20%, 30%, 50%, 70%, and 90% and 20%, 30%, 50%, 70%, and 90% of the maximum pixel values on the maps and are intended to display areas that may be cospatial with the CO as shown in the left panel.

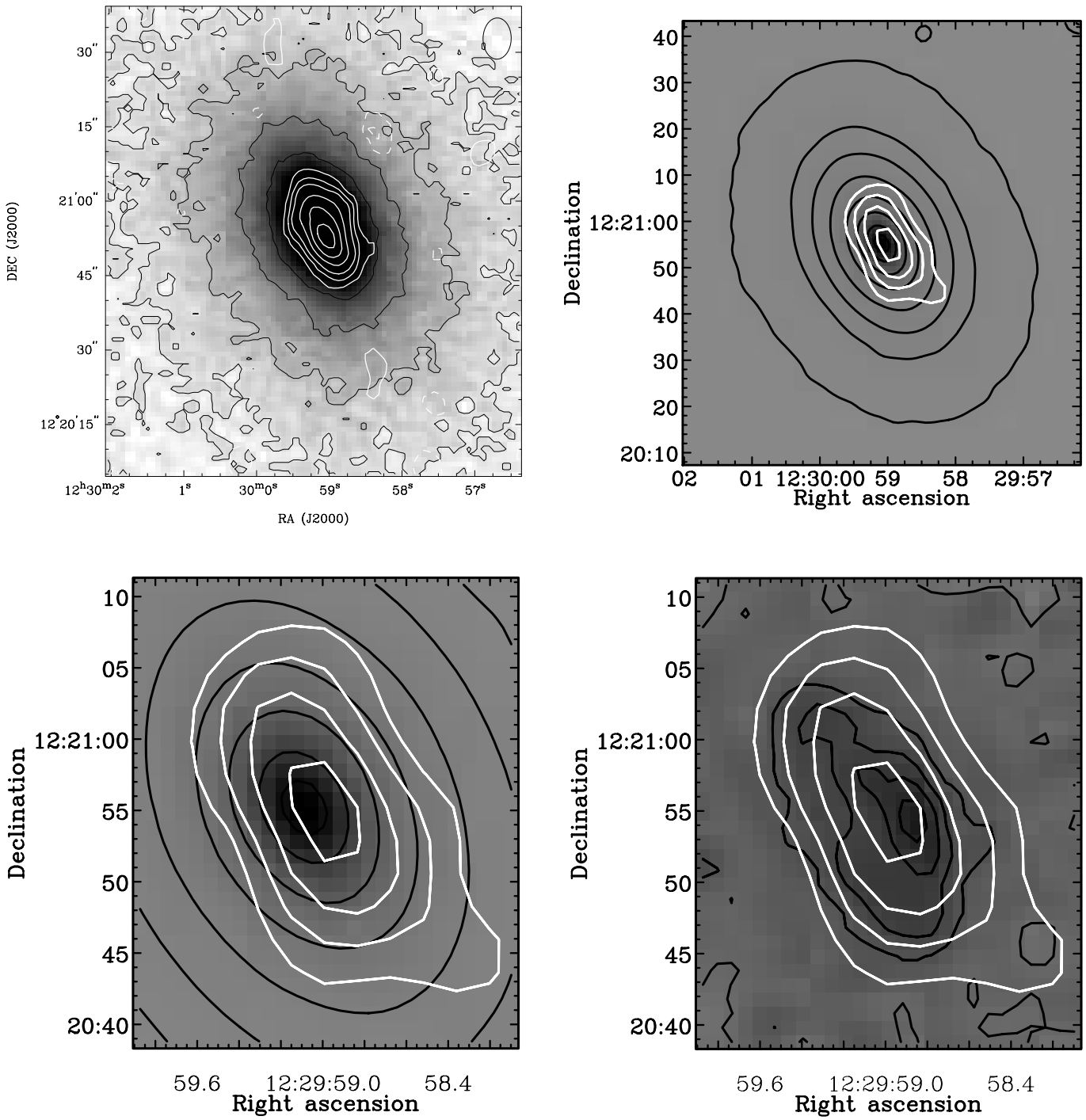

FIG. 7.— *Top left*: Total integrated CO(1–0) intensity map of NGC 4476 (*white contours*), with a measured 10% contour level diameter of 27″, overlaid on the gray scale and black contours from the red part of the optical DSS2, as presented by Young (2002). The white contours are in units of −20%, −10%, 10%, 20%, 30%, 50%, 70%, and 90% of 12.4 Jy beam^{-1} km s^{-1} = 7.3×10^{21} cm^{-2} CO peak (Young 2002). *Top right*: CSO/SHARC II 350 μm continuum smoothed to 10″ (*white contours*), overlaid on the intensity gray scale and black contours of the SDSS *i*-band image of NGC 4476 smoothed to 10″. The SDSS *i*-band and submillimeter contours are, respectively, ∼31%, 32%, 33%, 35%, 40%, 50%, 70%, and 90% and 30%, 50%, 70%, and 90% of the maximum pixel values on the maps and are intended to display areas that may be cospatial with the CO as shown in the top left panel. *Bottom left*: Zoom-in of the top right panel. *Bottom right*: CSO/SHARC II 350 μm continuum (*white contours*) smoothed to ∼10″, overlaid on the gray scale and black contours of the SDSS $i - g$–band images smoothed to 2″. The SDSS contours are on a linear scale, and the submillimeter contours are as above. In the SDSS $i - g$–band maps, darker pixels have redder colors.

NGC 3656 is probably in a thin, warped disk that provides the strongest extinction where the disk is tangent to the line of sight. In the center, the thin disk is therefore tangent to the line of sight and thus provides the strong optical extinction and submillimeter emission seen there, while it is more face-on or in the background in the western part of the galaxy. In the eastern part of the galaxy, the disk is either more edge-on or in the foreground and thus exhibits the moderate optical extinction seen there (see Fig. 1).

A thin, warped disk similar to that described for NGC 3656 has also been observed in another early-merger galaxy, Centaurus A (Leeuw et al. 2002; Quillen et al. 2006), showing extinction and submillimeter emission features similar to those seen in NGC 3656. In Centaurus A, it has been speculated that the disk has

TABLE 2
SHARC II and *IRAS* Continuum Fluxes for the Selected Elliptical Galaxies

Source	Peak at 350 μm (mJy per 9″ beam)	Total 350 μm (Jy)	Total 100 μm (Jy)	Total 60 μm (Jy)	Total 25 μm (Jy)	Total 12 μm (Jy)
NGC 3656	368 ± 73	0.69 ± 0.14	6.58 ± 0.68	2.54 ± 0.13	0.32 ± 0.03	0.14 ± 0.03
NGC 5666	150 ± 30	0.52 ± 0.10	3.98 ± 0.40	1.99 ± 0.10	0.16 ± 0.04	0.12 ± 0.04
NGC 83	191 ± 38	0.25 ± 0.05	2.15 ± 0.28	0.34 ± 0.09	<0.03	0.06 ± 0.02
NGC 759	71 ± 14	0.42 ± 0.08	2.36 ± 0.28	0.85 ± 0.06	0.07 ± 0.02	0.07 ± 0.03
NGC 807	63 ± 12	0.45 ± 0.09	1.83 ± 0.22	0.41 ± 0.03	0.12 ± 0.02	0.12 ± 0.03
UGC 1503	57 ± 11	0.24 ± 0.05	1.43 ± 0.20	0.40 ± 0.03	0.07 ± 0.03	<0.03
NGC 4476	117 ± 23	0.28 ± 0.06	1.84 ± 0.21	0.66 ± 0.05	<0.04	<0.05

formed from dust-rich material accreted from a merger that involved a gas-rich spiral galaxy (e.g., Quillen et al. 2006). The similarity of the warped dust disk together with the H I shells (Balcells et al. 2001) detected in NGC 3656 to those same features observed in Centaurus A suggests these two galaxies have a similar evolutionary history and that NGC 3656 may indeed be a younger, more distant analog of Centaurus A.

3.2. *The Intermediate-Age Merger/Accretion Elliptical NGC 5666*

The H I in NGC 5666 extends well beyond the optical galaxy; in addition, it is in circular orbits that indicate it is in dynamic equilibrium (Lake et al. 1987), since a not-too-recent (or intermediate-age) merger/accretion event is thought to have occurred in this galaxy (e.g., Donzelli & Davoust 2003). Using the Canada-France-Hawaii Telescope (CFHT), Donzelli & Davoust (2003) obtained optical CCD spectroscopy and imaging that revealed a "spiral" dusty structure with tidal tails and H II regions this galaxy. The spiral and tidal tails are revealed after subtracting a model of the bulge plus disk of the host galaxy.

Figure 2 shows that CO emission and submillimeter continuum contours of NGC 5666 follow each other in the high-brightness region greater than the 50% contour level. Outside the 10″ radius the CO emission contours are more north-south, while the submillimeter ones (which are not detected at a high signal-to-noise ratio) are east-west and slightly more extended than the CO. In the eastern part of the galaxy, the submillimeter and optical SDSS *i*-band contour levels follow each other down to the 30% level. However, in the western part, these contours only follow each other to the 70% level. The asymmetry in the contour correspondence supports the idea that the dust distribution or extinction in NGC 5666 is not even but, for example, in a spiral structure as suggested by Donzelli & Davoust (2003).

Figure 2 also shows a red extinction region within the 10″ diameter that coincides with the CO emission and submillimeter continuum peaks and the location of the spiral that was revealed in this galaxy by Donzelli & Davoust (2003). This extinction map also shows a patchy region outside a 15″ radius that may coincide with foreground dust patches or the location of the optical tidal tails connected to the spiral dusty structure.

3.3. *The Late-Merger/Accretion Ellipticals NGC 83 and NGC 759*

NGC 83 and NGC 759 are elliptical galaxies with surface brightness profiles that are fit by the $r^{1/4}$ law (e.g., Young 2005; Wiklind et al. 1997). Using deep CCD *V* and *R* images, Young (2005) confirmed in detail that NGC 83 is classically fit by the $r^{1/4}$ law from about radii 6″ to 80″ and that within about radii 6″ it has a regular-shaped cold gaseous dust disk. NGC 759 is also an elliptical galaxy in which Wiklind et al. (1997) earlier showed that there is a compact, star-forming, central, cold gaseous disk.

Consistent with dust-emitting components that are likely coincident with the compact gaseous disk detections in NGC 83 (Young 2005) and NGC 759 (Wiklind et al. 1997), both these galaxies are not resolved in the submillimeter images presented in Figures 3 and 4. The DSS2 blue and red optical images of these galaxies are saturated; here the $V - R$ extinction maps of Young (2005) are compared with SHARC II emission maps of the dust.

The central disks in NGC 83 and NGC 759 could represent a late stage in the merging of two disk galaxies or accretion of gas-rich material. The gas could have lost momentum in the merging process (or since the accretion) and fallen to the center of the galaxy. If this gas component is capable of forming stars, it could produce the high phase density characteristic of ellipticals.

TABLE 3
Intrinsic Galactic Sizes of the Stellar, Molecular Gas, and Dust Distributions

	50% 350 μm Flux		50% CO Flux		50% SDSS *i*-Band Flux[a]	
Source	arcsec	kpc	arcsec	kpc	arcsec	kpc
NGC 3656	6.5×12.7	1.5×2.8	2.6×13.2	0.5×2.8	11.2×17.3	2.4×3.8
NGC 5666	10.3×11.2	1.8×2.0	8.2×11.1	1.3×1.8	12.5×15	2.1×2.5
NGC 83	4.1×5.0	2.0×1.8	3.8×5.2	1.5×2.0	Saturated	Saturated
NGC 759	5.0×5.0	1.5×1.5	3.7×4.5	1.0×1.5	Saturated	Saturated
NGC 807	13.7×30.4	4.3×9.3	11.7×20.3	3.5×6.3	$20 \times 32^*$	$6.3 \times 9.8^*$
UGC 1503	12.1×21.4	4.0×7.0	9.4×15.2	3.0×5.0	$15.3 \times 18.9^*$	$5.0 \times 6.3^*$
NGC 4476	4.1×19.1	0.3×1.5	3.0×13.4	0.3×1.0	2.0×9.8	0.2×0.9

Notes.— At the 50% contour levels of the respective peak surface brightness. The listed SDSS *i*-band size for NGC 3656 is at the 70% contour level. See text for further details.

[a] An asterisk indicates the 50% DSS2 red flux was used instead.

3.4. *The Quiescent or Very Late Accretion Ellipticals UGC 1503 and NGC 807*

Of the ellipticals presented here, UGC 1503 and NGC 807 are the only objects that are (1) field galaxies and (2) have no currently identified optical morphological signatures of a merger or accretion event. Therefore, they are referred to as quiescent or very late accretion, meaning that if there has been any possible accretion event during their evolutionary lives, it happened a very long time ago, and the galaxies have now settled beyond any such event. Being field galaxies also means that there is no near neighbor that may have interacted with them in the recent past.

UGC 1503 and NGC 807 have intrinsic 50% contours of CO emission and 350 μm continuum fluxes that are comparable in extent to and only slightly smaller than those of the optical. These galaxies probably have dust that is distributed in slightly edge-on disks with their near side in the northeast and northwest for UGC 1503 and NGC 807, respectively. Young (2002) reports that in NGC 807, 70% of the CO emission is detected in the southern part of the galaxy (see Fig. 6), suggesting the bulk of the disk's content is in the southern part.

3.5. *The Accretion Virgo Cluster Dwarf Elliptical NGC 4476*

Despite directed searches, H I has not been detected in the cluster galaxy NGC 4476 (or NGC 759) (e.g., Lucero et al. 2005); this is in spite of CO gas detections in these galaxies (Lees et al. 1991; Wiklind & Henkel 1995; Wiklind et al. 1997; Young 2002). It is thought that the H I may have been destroyed by the hot cluster gas or, in the case of NGC 4476, by ram pressure stripping (Lucero et al. 2005).

Using *HST V* (F555W) imaging, van Dokkum & Franx (1995) showed that NGC 4476 has a regular, "spiral-like" dust lane that is about 20″ in diameter. They determined a difference of 19° between the major-axis position angle of the dust lane and that of the stellar component and used the evidence in this and a sample of other early galaxies to argue that the dust lane in NGC 4476 did not originate from the stellar component but was instead *externally accreted*. Tomita et al. (2000) confirmed the existence of the regular dust lane using *HST E*($V - I$) (F555W − F814W) extinction images and showed that NGC 4476 has H II regions. They also noted a blue unresolved nucleus that they suggested might come from a young star cluster(s) associated with the dust system. Young (2002) detected CO gas in a relaxed disk that is cospatial with the dust lane and has a diameter of about 27″.

Figure 7 shows 350 μm continuum contours of dust emission from NGC 4476 that generally follow the direction of the ellipticity and major-axis position angle of those of the CO disk and SDSS extinction maps, except at parts of the 350 μm continuum at 30% flux levels. In the eastern part of the galaxy, the 70%, 50%, and 30% contour levels of the SDSS *i*-band and SHARC II 350 μm (of the stellar and dust components, respectively) intensities coincide quite well. The SDSS extinction image in this region extends to the 30% SHARC II 350 μm contour level. However, in the western part of the galaxy, the correspondence of the contours levels is not so good, suggesting that the dust and stellar disks are not in the same plane. Indeed, the SDSS color map shows less extinction in the western part of the galaxy, as may be the case if the dust disk is toward the background or inner parts of the galaxy in that region. The 350 μm continuum 50% contour levels along the major axis of the galaxy are more extended than the CO and stellar intensities of the same relative levels. These results suggest that the dust component is separate from the stellar one, as concluded by van Dokkum & Franx (1995) from their *HST* data of the central region in this galaxy. The 350 μm continuum 30% contour levels (which are not detected at a high signal-to-noise ratio) are also more extended than the CO and extinction ones and have a spur in the southwest. This emission spur may be part of the dust disk in the eastern background of the galaxy.

The H II regions in NGC 4476 (and NGC 5666) probably obtain their fuel from the dust seen in both the optical extinction and submillimeter and in turn heat the dust to produce the FIR-submillimeter emission seen in these galaxies. Further discussion of star formation, the heating mechanisms, and the dust sources is given in § 5 and will subsequently be analyzed in more detail in a follow-up paper that uses *Spitzer* mid-infrared (MIR) spectroscopy of these galaxies (L. L. Leeuw et al., in preparation).

4. THE MIR-TO-SUBMILLIMETER SPECTRAL ENERGY DISTRIBUTION AND LUMINOSITIES

The MIR flux in ellipticals comes primarily from "warm" galactic dust, nebulae, or the envelopes of evolved stars, while the FIR-to-submillimeter flux comes mainly from cold dust with temperatures $T \lesssim 100$ K; in the case of radio-bright sources, it can also originate from the high-frequency radio components. On the other hand, flux in the optical/near-IR comes primarily from the stellar components of $T \gtrsim 1000$ K, with negligible contribution to the FIR-to-submillimeter spectrum. For the radio-faint sources observed in this program, it is assumed that the MIR-to-submillimeter SED emission comes from a cold-to-cool (5 K $\lesssim T \lesssim$ 100 K) thermal component plus a MIR power-law component that includes PAHs, warm ($T \gtrsim 100$ K) dust, and stellar galactic components.

Motivated by the general appearance of the SEDs of the elliptical galaxies and the available data, the SED is modeled with a power law in the MIR (8–40 μm) and a graybody in the FIR (40–2000 μm). The mid-IR power-law fit is not a physical model but rather a mathematical tool to aid in the calculation of total MIR luminosity for the galaxies. However, the graybody fit is an attempt at physically modeling the average temperature, emissivity, and optical depth of the cold dust emission for the galaxies.

The model fits are plotted in Figure 8, where their derived parameters are labeled, and listed in Table 4. The power-law model is generated with a truncated F_ν temperature distribution, thus the shape of the MIR components shown in the SED plots. For sources which have less than two measurements in the MIR, the median power law $F_\nu^{\sim -0.4}$ is assumed. The power law for NGC 4476, which has no MIR detection, shows a 3 σ upper limit in Figure 8. Reasonable temperature and β are derived for the graybody part of the spectrum for all sources except NGC 83. For that source, it is assumed that the dust emissivity index β is equal to the median value of 1.8.

Cold dust temperatures and emissivity indices are determined to be in the range 23 K $\lesssim T \lesssim$ 31 K and $1.5 \leq \beta \leq 2.2$, respectively, for the sample. These parameters are typical for single-graybody fits to unresolved FIR-to-submillimeter fluxes of dust emitting from elliptical galaxies (e.g., Leeuw et al. 2004; Temi et al. 2004). However, they are about 7° cooler than the dust temperatures of ellipticals derived from 60 and 100 μm flux ratios alone and a fixed $\beta = 1.0$ (e.g., Wiklind et al. 1995). On the other hand, the dust temperatures are also slightly warmer and the emissivity indices similar to those of dust in the Milky Way and nearby spiral galaxies (e.g., Dunne et al. 2000).

The cold dust continuum emission presented here extends over 10 kpc for some galaxies in the sample, is detected at high signal-to-noise ratio with SHARC II, and is generally cospatial with previously imaged CO emission (see, e.g., § 3). Above the 50% contour levels, the submillimeter dust continuum and optical

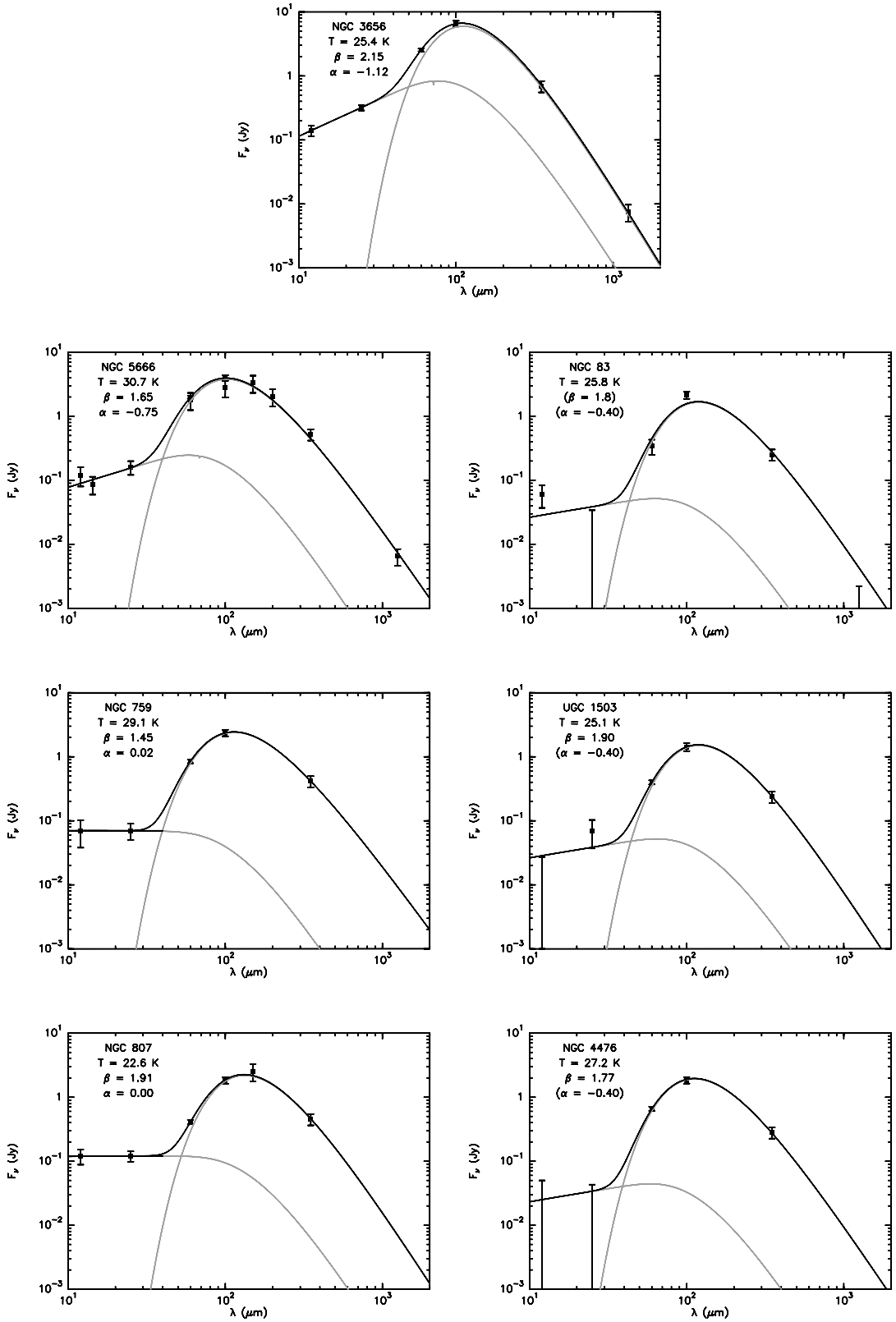

FIG. 8.—CSO/SHARC II 350 μm continuum integrated fluxes and MIR-to-submillimeter data obtained from public archives and the literature (see Table 2) for the sample galaxies, plotted and fitted with a composite model of a single-temperature graybody plus MIR power law (see § 4).

stellar intensities of similar spatial resolution have the same general distribution, suggesting that the dust, CO, and stellar components in the central regions are all cospatial. The early-merger elliptical NGC 3656, with its disturbed optical morphology, is an exception to this coupling of submillimeter and optical central flux distributions.

The current maps are not detected at high enough significance that proper dust distributions can be discerned below the 30% contour levels. If there exists any dust component for the sample that is cooler or has lower level emission that perhaps extends over the entire galactic stellar or H I distributions (see, e.g., § 5),

TABLE 4
MIR to SHARC II–derived Cold Dust Parameters and Related Gas Properties

Source	T (K)	β	$M(d)$ ($10^6\ M_\odot$)	$M(H_2)/M(d)$	$M(H_2 + H\ I)/M(d)$
NGC 3656.....	25.4	2.2	15	313	387
NGC 5666.....	30.7	1.6	4.8	119	327
NGC 83.....	25.8	(1.8)	19	105	...
NGC 759.....	29.1	1.5	15	160	<320
NGC 807.....	22.6	1.9	25	56	300
UGC 1503.....	25.1	1.9	12	150	283
NGC 4476.....	27.2	1.8	0.9	122	<233

TABLE 6
The Optical Depth and Total FIR and CO Star Formation Rate Estimates

Source	350 μm Peak $\tau_{optical}$	A_V	Total FIR SFR ($M_\odot\ yr^{-1}$)	Total CO SFR ($M_\odot\ yr^{-1}$)
NGC 3656.....	0.00119	17	3.04	26.89
NGC 5666.....	0.00050	7	1.17	1.17
NGC 83.....	0.00171	24	2.65	6.13
NGC 759.....	0.00206	29	2.41	10.38
NGC 807.....	0.00018	25	2.17	1.73
UGC 1503.....	0.00015	2	1.44	2.83
NGC 4476.....	0.00047	7	0.14	0.28

its detection will have to await the next-generation submillimeter detectors, such as those on ALMA, *Herschel*, JCMT, and SOFIA. Combining the current data set with anticipated *Spitzer* and other upcoming sensitive FIR-to-submillimeter observations and analyzing the SEDs of mapping data from various FIR-to-submillimeter bands should put tighter constraints on the physical parameters of cold dust in the sample.

MIR-to-submillimeter luminosities ($L_{0.04-1\ mm}$ and $L_{8\ \mu m-1\ mm}$) that were obtained by integrating below the model fits shown in Figure 8 are listed in Table 5, and these can be compared to the optical luminosities (L_B) that are also listed in Table 5. The percentage excess MIR-to-submillimeter luminosities over the total luminosities ($L_{B-1\ mm}$) are determined and also listed in Table 5. For most of the galaxies, the MIR-to-submillimeter excess luminosities are about 20%–30% of the total luminosities, with about 70% or more of the excess emitted at FIR-to-millimeter wave bands as thermal cold dust emission (see Fig. 8 and Table 5). The respectively early-age and intermediate-age galaxies NGC 3656 and NGC 5666 have higher-than-average MIR-to-submillimeter excesses of the total luminosities ($\gtrsim$50%) for the sample (see Table 5), suggesting more or denser dust and star formation or, at least, fairly high MIR-to-submillimeter emission in comparison to total emission in these more recent merger remnant/dust accretion galaxies.

5. ESTIMATES OF STAR FORMATION RATES AND OTHER LUMINOSITY SOURCES

The peak 350 μm optical depths given in Table 6 were determined using the 350 μm continuum fluxes and intrinsic 350 μm sizes presented in Tables 2 and 3, respectively, for each galaxy. According to Draine (2003), the corresponding peak optical extinctions are about 14,000 times larger than the submillimeter optical depth values, implying peak visual extinctions (A_V) greater than 2 mag for all the galaxies in the sample. Therefore, the dust measured at 350 μm for these galaxies is dense enough to absorb almost all the UV or optical radiation emitted by any massive star embedded within it.

TABLE 5
MIR-to-Millimeter Luminosity Excess

Source	$L_{0.04-1\ mm}$ ($10^9\ L_\odot$)	$L_{8\ \mu m-1\ mm}$ ($10^9\ L_\odot$)	$L_{B-1\ mm}$ ($10^9\ L_\odot$)	$\%L_{B-1\ mm}$ as $L_{8\ \mu m-1\ mm}$	$\%L_{B-1\ mm}$ as $L_{0.04-1mm}$
NGC 3656.....	14.0	17.8	33.8	53	41
NGC 5666.....	5.4	6.8	12.8	53	42
NGC 83.....	11.7	13.8	57.8	24	20
NGC 759.....	10.9	13.8	47.8	29	23
NGC 807.....	8.1	12.6	43.6	29	18
UGC 1503.....	6.9	8.3	24.3	34	28
NGC 4476.....	0.6	0.7	3.7	19	16

If the FIR luminosity, L_{FIR}, for each galaxy in our sample is due to the reprocessing of radiation from embedded, newly formed stars, then an estimate can be made of the current star formation rate (SFR) in each galaxy using the relation given in Kennicutt (1998),

$$\mathrm{SFR}\ M_\odot\ \mathrm{yr}^{-1} = 1.75 \times 10^{-10} L_{FIR}\ L_\odot, \quad (1)$$

where L_{FIR} includes radiation from 8 to 1000 μm. Table 5 lists the estimate of L_{FIR} for each galaxy based on the fits to the data shown in Figure 8. Except for NGC 4476, equation (1) yields SFR estimates ranging from 1 to 3 $M_\odot\ yr^{-1}$ for the galaxies in the sample (see Table 6). These rates are similar to the SFR in the Milky Way, a spiral galaxy, but are about 10 times those for "normal" elliptical galaxies. NGC 4476 has a SFR estimate more in line with that of a normal elliptical galaxy. However, NGC 4476 is exceptional in this sample in that it is a dwarf elliptical near the center of the Virgo Cluster.

For the most part, the FIR luminosity given in Table 5 for each galaxy is composed of power radiating at wavelengths longer than 40 μm. Based on the SEDs shown in Figure 8, the majority of this FIR power, therefore, could be coincident with the 350 μm emission, which seems to be embedded in rotating CO "disks." Thus, the FIR data and our 350 μm data imply, for most of the galaxies in our sample, the presence of ministarbursts inside central rotating disks of gas and dust.

There is another, more indirect way to estimate SFR, by using the empirical relationship from Kennicutt (1998) between SFR surface density, SD_{SFR}, and the molecular gas surface density, SD_{gas}:

$$SD_{SFR}\ M_\odot\ \mathrm{yr}^{-1}\ \mathrm{kpc}^{-2} = 2.5 \times 10^{-4} \left(SD_{gas}\ M_\odot\ \mathrm{pc}^{-2}\right)^{1.4}. \quad (2)$$

Estimates of the SFR surface densities at the peaks of the gas distributions in these galaxies have been derived based on the total molecular gas masses (Table 1) and the intrinsic sizes of the CO distributions in these galaxies (Table 3). The product of the SFR surface densities with the intrinsic areas of the CO distributions yield the total SFRs for the galaxies, and these are listed in Table 6.

A comparison between the SFR values estimated using the two methods given above would imply that NGC 759 and, especially, NGC 3656 have the potential (in gas) for considerably more star formation than is currently being observed in the FIR, but that the other galaxies in our sample are using their gas reservoirs at about the "normal" rate to form stars.

The discussion above assumes that the FIR excess from these galaxies originates from star formation; however, as noted in § 1, Mathews & Brighenti (2003) argue that the FIR excess could be

due to the thermal energy released by the hot ISM as it cools through thermal electron collisions with dust grains. In this scenario, the central cold dust seen in these elliptical galaxies originates from the settling of the cooled hot dusty gas from mass-losing red giants distributed throughout each of the elliptical galaxies, rather than from the gas and dust from recent galaxy merger or accretion events. Mathews & Brighenti (2003) estimated the FIR luminosity radiated from the dust grains involved in the cooling of the hot gas of about 10^7 K for a given total stellar mass-loss rate, $\dot{M}/M_\odot$ yr^{-1}, to be approximately

$$L_{\rm FIR}\ L_\odot \sim 5.1\times10^7\left(T/10^7\ {\rm K}\right)\dot{M}/M_\odot\ {\rm yr}^{-1}. \quad (3)$$

Substituting the FIR luminosity listed for each galaxy in Table 5 gives mass-loss rates ranging from 15 to 340 $M_\odot$ yr^{-1} for this set of galaxies. These rates are much higher than those for giant elliptical galaxies, which are normally $\sim$1 $M_\odot$ yr^{-1}. The larger mass-loss rates seem consistent with the larger-than-normal dust masses at the center of these galaxies as implied by our 350 μm data; however, the optical/near-IR luminosity for each galaxy in the sample presented here is similar to normal giant elliptical galaxy optical/near-IR luminosities, so normal stellar mass-loss rates would be expected for these galaxies. Hence, although both the FIR luminosity and the 350 μm dust mass estimates are consistent with large stellar mass-loss rates for the galaxies in this sample, the optical/near-IR luminosities for these galaxies are not consistent with such a stellar mass-loss increase.

In summary, the calculations given in this section favor the FIR luminosity of these galaxies resulting primarily from cold dust in the central currently star-forming regions that were probably induced and supported by accretion or merger events involving a gas- or dust-rich galaxy or satellite, rather than coming from hot ISM cooling in collisions with dusty gas from stellar mass loss. However, a small FIR luminosity contribution from the hot ISM cooling or from the stellar or any other dilute galactic radiation field is not excluded.

6. DUST MASSES AND GAS-TO-DUST MASS RATIOS

Following Hildebrand (1983), the mass of dust, M_d, that emits MIR-to-submillimeter continuum can be estimated from

$$M_d = \frac{F_\nu D^2}{k_d B(\nu, T)}, \quad (4)$$

where F_ν is the measured flux density at frequency ν, D is the distance to the source, $B(\nu, T)$ is the Planck function, and $k_d = 3Q_\nu/4a\rho$ is the grain mass absorption coefficient, where a and ρ are the grain radius and density, respectively. A recently updated value of $k_d^{350\ \mu{\rm m}} = 1.92\times10^{-1}$ m^2 kg^{-1} (Draine 2003), as for Galactic dust, is assumed, yielding dust masses that range from $\sim9\times10^5$ to $\sim2.5\times10^7$ $M_\odot$ for dust with temperatures in the range 23 K $\lesssim T \lesssim$ 31 K (see Fig. 8 and Table 4).

NGC 4476 has the lowest dust mass in the sample. The relative paucity of dust in this galaxy is not surprising, as NGC 4476 is a dwarf elliptical. However, Lucero et al. (2005) observed that this galaxy, which lies within the Virgo Cluster, has been stripped of its H I, possibly through ram pressure; therefore, the presence of any compact distribution of CO and cold dust implies that H I is more vulnerable to ram pressure stripping than is the denser molecular gas and the dust associated with it within this cluster galaxy.

Table 4 shows that the sample has diverse H_2 mass–to–dust mass ratios that are mostly in the range $120 \lesssim M(H_2)/M_{\rm dust} \lesssim 160$ and, in the quiescent galaxy NGC 807 and early-merger remnant NGC 3656, range from $\sim$60 (about half the average) to $\sim$310 (about twice the average), respectively. The ratios suggest that, in the central galactic regions where the H_2 and dust masses are measured from the resolved CO and our CSO continuum measurements, respectively, some of the sample galaxies are relatively undermassive in H_2 and overmassive in dust content, while the others are overmassive in H_2 and undermassive in dust content. The implications of these mass ratios and their possible association with star formation or, at least, gas phases in the central regions of these galaxies will be investigated further in our upcoming paper that uses *Spitzer* IRS data to study the MIR spectral evolution and/or star formation properties of these galaxies.

The total cold gas mass [i.e., (H_2 + H I) mass]–to–dust mass ratios for the sample are, however, less diverse and in a narrower range of $230 \lesssim M(H_2 + {\rm H\ I})/M_{\rm dust} \lesssim 400$, with NGC 807 and NGC 3656 at much closer ratios of 300 and 387, respectively (see Table 4). At face value, it may appear that the total cold gas mass–to–dust mass ratio for the sample is about 3 times the value for the Milky Way [i.e., $M(H_2 + {\rm H\ I})/M_{\rm dust} \sim 100$]. However, in sample objects where H I has been resolved (e.g., Lake et al. 1987; Balcells et al. 2001), the atomic gas has been observed to be much more extended than the inner galactic regions where our observations have mapped dust emission and shown it to be associated with molecular gas. A cold and extended dust component may yet be detected that is associated with atomic hydrogen and perhaps massive enough to bring the total cold gas–to–dust mass ratio for the sample in line with the Milky Way value.

7. SUMMARY OF RESULTS AND CONCLUSIONS

SHARC II continuum observations at 350 μm of seven elliptical galaxies with known CO gas disks have been presented (Wiklind et al. 1997; Young 2002, 2005). The SHARC II mapping provides the first *clearly resolved* FIR-to-submillimeter continuum emission from cold dust (with temperatures $\sim$31 K $\gtrsim T \gtrsim$ 23 K) of any elliptical galaxy >40 Mpc. Calculations of the measured FIR excess show that the dust's most likely and dominant heating source is not dilute stellar radiation or cooling flows, but rather star formation that could have been triggered by an accretion or merger event and fueled by dust-rich material that has settled in a dense region cospatial with the central CO gas disks. The dust is detected even in two cluster ellipticals that are deficient in H I, showing that, unlike the H I, cold dust and CO in ellipticals can survive among hot X-ray gas, even in galaxy clusters.

Above the 50% contour levels, where the submillimeter detections are of high significance, the submillimeter dust continuum and optical stellar intensities of similar spatial resolution have the same general distribution, suggesting that the dust, CO, and stellar components in the central regions are cospatial. The early-merger elliptical NGC 3656, with its dense optical dust lane that is thought to be in a highly inclined warped disk, is an exception to this coupling of submillimeter and optical central flux distributions. Below the 50% contour levels, and especially below the 30% levels, the current maps are not detected at high enough significance that proper dust distributions can be discerned.

No dust cooler than 20 K, distributed outside the CO disks, or cospatial with and heated by the entire dilute stellar optical galaxy (or very extended H I) is currently evident. These observations clearly show that the FIR-submillimeter emission in our sample ellipticals is primarily from cold dust that is associated with star formation located in the central parts of these galaxies. The results support the hypothesis that if ellipticals are formed through mergers of gas-rich spirals, their starbursts (1) are necessary to produce the high phase-space density seen in the center of

ellipticals and (2) would power the FIR-bright stage as the merger relaxes. Combining the current data set together with anticipated *Spitzer* and other upcoming sensitive FIR-to-submillimeter mapping observations may detect or rule out the existence of larger scale, diffusely distributed cold dust with an average temperature that is perhaps <20 K (and maybe associated with H I).

Assuming the grain mass absorption coefficient $k_d^{350\,\mu\mathrm{m}} = 1.92 \times 10^{-1}\ \mathrm{m^2\,kg^{-1}}$, as for Galactic-like dust (Draine 2003), the measured submillimeter fluxes and dust temperatures yield dust masses for the sample that range from $\sim 9 \times 10^5$ to $\sim 2 \times 10^7\ M_\odot$. The sample has diverse H_2 mass–to–dust mass ratios that cover $60 \lesssim M(\mathrm{H_2})/M_{\mathrm{dust}} \lesssim 310$, suggesting that in the central galactic regions, where the H_2 and dust masses are measured from the resolved CO and our CSO/SHARC II continuum measurements, respectively, some of the sample galaxies are relatively undermassive in H_2 and overmassive in dust content, while others are the opposite. The possible implications of these mass ratios on star formation or, at least, gas phases in the central regions of these galaxies will be investigated further in our upcoming paper that uses *Spitzer* IRS data to study the detailed MIR spectral and/or star formation properties of these galaxies.

The total cold gas mass–to–dust mass ratios for the sample are in a narrower range of $230 \lesssim M(\mathrm{H_2} + \mathrm{H\ I})/M_{\mathrm{dust}} \lesssim 400$, with a total cold gas mass–to–dust mass ratio for the sample that, at face value, may appear to be about 3 times the value for the Milky Way (i.e., $\sim$100). However, in sample objects where atomic gas has been resolved (e.g., Lake et al. 1987; Balcells et al. 2001), the H I has been observed to be much more extended than the inner galactic regions where our observations have mapped dust emission that is associated with molecular gas. A cold and extended dust component that is associated with atomic hydrogen may yet be detected and may be massive enough to bring the total cold gas–to–dust mass ratio for the sample in line with the Milky Way value. As noted above, this may be observed with future, more sensitive FIR/submillimeter detectors, such as those on SOFIA, *Herschel*, JCMT, or ALMA.

Part of the research described in this paper was carried out at the Jet Propulsion Laboratory, California Institute of Technology, under a contract with the National Aeronautics and Space Administration (NASA). Part of the research was carried out while L. L. L. was at the University of Chicago and partially supported by a Chicago 2004 NASA Mini-Award Grant and National Science Foundation (NSF) grant AST 05-05124. L. L. L. wrote this paper while supported by the South Africa Square Kilometre Array/MeerKAT at Rhodes University and finalized it at NASA Ames Research Center. Research at the Caltech Submillimeter Observatory is supported by NSF grant AST 05-40882.

This publication makes use of data products from the second Digital Sky Survey (DSS2), which was based on photographic data obtained using the Oschin Schmidt Telescope on Palomar Mountain. The Palomar Observatory Sky Survey was funded by the National Geographic Society. The Oschin Schmidt Telescope is operated by the California Institute of Technology and Palomar Observatory. The plates were processed into the present compressed digital format with their permission. The DSS was produced at the Space Telescope Science Institute under US Government grant NAG W-2166.

REFERENCES

Athey, A., Bregman, J., Bregman, J., Temi, P., & Sauvage, M. 2002, ApJ, 571, 272
Balcells, M. 1997, ApJ, 486, L87
Balcells, M., van Gorkom, J. H., Sancisi, R., & del Burgo, C. 2001, AJ, 122, 1758
Barnes, J. E. 2002, MNRAS, 333, 481
Donzelli, C. J., & Davoust, E. 2003, A&A, 409, 91
Draine, B. T. 2003, ARA&A, 41, 241
Dunne, L., Eales, S., Edmunds, M., Ivison, R., Alexander, P., & Clements, D. L. 2000, MNRAS, 315, 115
Goudfrooij, P., & de Jong, T. 1995, A&A, 298, 784
Hildebrand, R. H. 1983, QJRAS, 24, 267
Kennicutt, R. C., Jr. 1998, ARA&A, 36, 189
Knapp, G., Guhathakurta, P., Kim, D., & Jura, M. 1989, ApJS, 70, 329
Knapp, G. R., & Patten, B. M. 1991, AJ, 101, 1609
Knapp, G. R., Turner, E. L., & Cunniffe, P. E. 1985, AJ, 90, 454
Lake, G., Schommer, R. A., & van Gorkom, J. H. 1987, ApJ, 314, 57
Lees, J. F., Knapp, G. R., Rupen, M. P., & Phillips, T. G. 1991, ApJ, 379, 177
Leeuw, L. L., Hawarden, T. G., Matthews, H. E., Robson, E. I., & Eckart, A. 2002, ApJ, 565, 131
Leeuw, L. L., Sansom, A. E., Robson, E. I., Haas, M., & Kuno, N. 2004, ApJ, 612, 837
Lucero, D. M., Young, L. M., & van Gorkom, J. H. 2005, AJ, 129, 647
Mathews, W. G., & Brighenti, F. 2003, ApJ, 590, L5
Murray, C. M., Oosterloo, T. A., & Morganti, R. 2000, BAAS, 32, 1591
Quillen, A. C., Brookes, M. H., Keene, J., Stern, D., Lawrence, C. R., & Werner, M. W. 2006, ApJ, 645, 1092
Rothberg, B., & Joseph, R. D. 2004, AJ, 128, 2098
———. 2006, AJ, 132, 976
Sadler, E. M., & Gerhard, O. E. 1985, MNRAS, 214, 177
Schweizer, F. 1998, in Saas-Fee Advanced Course 26, Galaxies: Interactions and Induced Star Formation, ed. R. C. Kennicutt, Jr., et al. (Berlin: Springer), 105
Seaquist, E. R., & Clark, J. 2001, ApJ, 552, 133
Temi, P., Brighenti, F., Mathews, W., & Bregman, J. 2004, ApJS, 151, 237
Tomita, A., Aoki, K., Watanabe, M., Takata, T., & Ichikawa, S.-I. 2000, AJ, 120, 123
Toomre, A., & Toomre, J. 1972, ApJ, 178, 623
Tran, H. D., Tsvetanov, Z., Ford, H. C., Davies, J., Jaffe, W., van den Bosch, F. C., & Rest, A. 2001, AJ, 121, 2928
van Dokkum, P. G., & Franx, M. 1995, AJ, 110, 2027
Wiklind, T., Combes, F., & Henkel, C. 1995, A&A, 297, 643
Wiklind, T., Combes, F., Henkel, C., & Wyrowski, F. 1997, A&A, 323, 727
Wiklind, T., & Henkel, C. 1995, A&A, 297, L71
Young, L. M. 2002, AJ, 124, 788
———. 2005, ApJ, 634, 258